The 2010 Haiti earthquake: A complex fault pattern constrained by seismologic and tectonic observations

Bernard Mercier de Lépinay,[1] Anne Deschamps,[1] Frauke Klingelhoefer,[2] Yves Mazabraud,[3] Bertrand Delouis,[1] Valérie Clouard,[4] Yann Hello,[1] Jacques Crozon,[2] Boris Marcaillou,[3] David Graindorge,[5] Martin Vallée,[1] Julie Perrot,[5] Marie-Paule Bouin,[6] Jean-Marie Saurel,[4] Philippe Charvis,[1] and Mildor St-Louis[7]

Received 30 September 2011; revised 14 October 2011; accepted 16 October 2011; published 18 November 2011.

[1] After the January 12, 2010, Haiti earthquake, we deployed a mainly offshore temporary network of seismologic stations around the damaged area. The distribution of the recorded aftershocks, together with morphotectonic observations and mainshock analysis, allow us to constrain a complex fault pattern in the area. Almost all of the aftershocks have a N-S compressive mechanism, and not the expected left-lateral strike-slip mechanism. A first-order slip model of the mainshock shows a N264°E north-dipping plane, with a major left-lateral component and a strong reverse component. As the aftershock distribution is sub-parallel and close to the Enriquillo fault, we assume that although the cause of the catastrophe was not a rupture along the Enriquillo fault, this fault had an important role as a mechanical boundary. The azimuth of the focal planes of the aftershocks are parallel to the north-dipping faults of the Transhaitian Belt, which suggests a triggering of failure on these discontinuities. In the western part, the aftershock distribution reflects the triggering of slip on similar faults, and/or, alternatively, of the south-dipping faults, such the Trois-Baies submarine fault. These observations are in agreement with a model of an oblique collision of an indenter of the oceanic crust of the Southern Peninsula and the sedimentary wedge of the Transhaitian Belt: the rupture occurred on a wrench fault at the rheologic boundary on top of the under-thrusting rigid oceanic block, whereas the aftershocks were the result of the relaxation on the hanging wall along pre-existing discontinuities in the frontal part of the Transhaitian Belt. **Citation:** Mercier de Lépinay, B., et al. (2011), The 2010 Haiti earthquake: A complex fault pattern constrained by seismologic and tectonic observations, *Geophys. Res. Lett.*, *38*, L22305, doi:10.1029/2011GL049799.

1. Introduction

[2] Aftershock recording is important to answer questions on the size and geometry of a ruptured area and on the state of stress in the epicentral area after an earthquake, and to more accurately define the epicenter location. However, the January 12, 2010, Haiti earthquake occurred in a poorly instrumented region that is located on a complex, wide, deformed zone on the boundary between the Caribbean Plate and the North-American Plate (Figure 1a). The area affected by this event lies on the eastern tip of the Southern Peninsula of Haiti, just on top of the connecting area of two major crustal structures: 1) the Enriquillo-Plantain Garden Fault Zone (EPGFZ), a left-lateral strike-slip fault that runs across the Southern Peninsula of Haiti; and 2) the Transhaitian Belt, a southwestward fold-and-thrust system on the southern edge of the main Hispaniola Block [*Pubellier et al.*, 2000]. The last significant earthquakes in this area occurred just over 240 years ago, in 1751 and 1770, when two large events with estimated magnitudes ≥7 struck the same area. As the EPGFZ shows evidence of ruptures during the Holocene, this fault zone was commonly regarded as responsible for the historical seismicity in this area. However, there is no evidence of surface rupture along the EPGFZ during this January 12, 2010, earthquake [*Prentice et al.*, 2010, *McHugh et al.*, 2011]. Global positioning system (GPS) studies show that the Caribbean Plate is moving at about 20 ± 3 mm.yr^{-1} east-northeastward (N70°E) relative to the North-American Plate, obliquely to the nearly E-W plate boundary [*Mann et al.*, 2002; *Calais et al.*, 2002, 2010]. This oblique convergence is decoupled into components of near strike-slip and thrust. The strike-slip component is mainly concentrated along the Septentrional Fault of Hispaniola for 9 ± 2 mm.yr^{-1} and the EPGFZ for 7 ± 2 mm.yr^{-1} [*Manaker et al.*, 2008]. The thrust component is about 4 mm.yr^{-1} [*Calais et al.*, 2010], and this is mainly at the northern edge of the plate boundary zone by the offshore North Hispaniola thrust zone and at the southern edge of the plate boundary zone by the offshore Muertos thrust zone and its on-land westward prolongation, the Transhaitian Belt [*Pubellier et al.*, 2000]. A better understanding of the rupture process and the stress relaxation of the 2010 Haiti earthquake is required for seismic risk assessment in this area, for which the recording of the aftershocks as soon as possible after the earthquake was essential.

2. Data Acquisition

[3] Given the peculiar geographic position of the affected area on the narrow Southern Peninsula of Haiti, we chose to deploy a sub-marine seismological network around the Peninsula to monitor the aftershock activity without interfering with humanitarian relief efforts. During the marine

[1]Géoazur, CNRS, Université de Nice, IRD, Valbonne, France.
[2]Géosciences Marines, Ifremer, Plouzané, France.
[3]IUFM de Guadeloupe, Université des Antilles et de la Guyane, Pointe-à-Pître, Guadeloupe.
[4]Observatoire Volcanologique et Sismologique de la Martinique, Institut de Physique du Globe de Paris, Fonds-St-Denis, Martinique.
[5]IUEM, Université de Bretagne Occidentale, Plouzané, France.
[6]Observatoire Volcanologique et Sismologique de la Guadeloupe, Institut de Physique du Globe de Paris, Gourbeyre, Guadeloupe.
[7]Bureau des Mines et de l'Energie, Port-au-Prince, Haiti.

Copyright 2011 by the American Geophysical Union.
0094-8276/11/2011GL049799

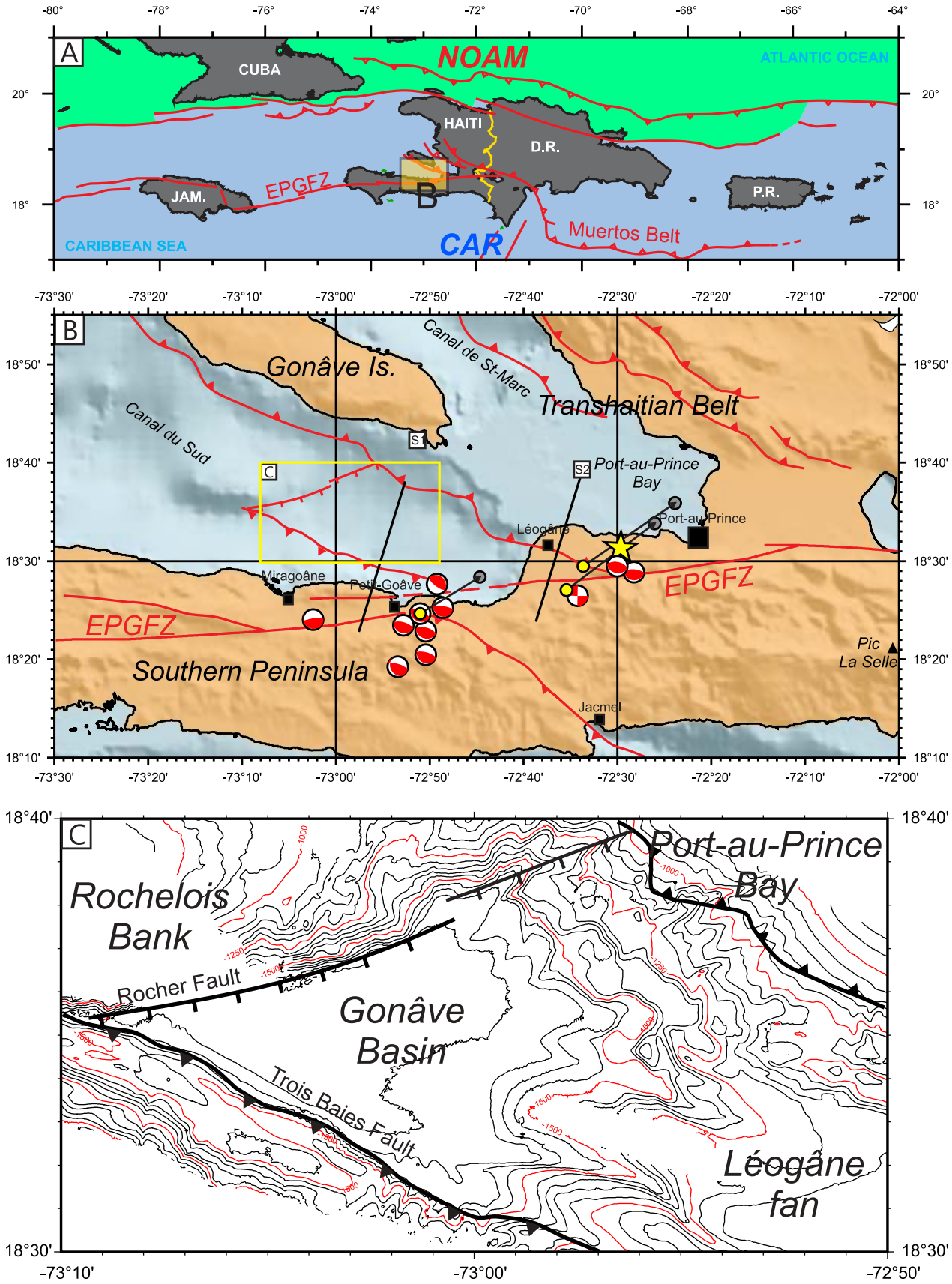
A
CUBA
NOAM
ATLANTIC OCEAN
HAITI
D.R.
JAM.
EPGFZ
B
P.R.
CARIBBEAN SEA
CAR
Muertos Belt
B
Gonâve Is.
Canal de St-Marc
Transhaitian Belt
Canal du Sud
S1
S2
C
Port-au-Prince Bay
Port-au-Prince
Léogâne
Miragoâne
Petit-Goâve
EPGFZ
EPGFZ
Pic La Selle
Southern Peninsula
Jacmel
C
Rochelois Bank
Port-au-Prince Bay
Rocher Fault
Gonâve Basin
Trois Baies Fault
Léogâne fan

Figure 1

scientific cruise of HAITI-OBS of the R/V L'Atalante, we deployed 21 ocean-bottom seismometers (OBS) in the Haitian waters around the epicentral area, on February 10 and 11, 2010. The spatial distribution of the marine instruments was strongly controlled by the bathymetry, and we avoided Port-au-Prince Bay, where the water is too shallow. Therefore, to complement the eastern part of the fault-zone area, we also deployed four onshore seismic stations. The OBS were four-component instruments, including a 2 Hz hydrophone, while the land stations were six-component instruments, including a three-component strong-motion accelerometric seismometer. Part of the OBS network (15 short-period instruments) was recovered on March 8 and 9, 2010, after three weeks of recording, the rest (Geoazur Hippocampe OBS, broadband) was recovered on May 15 and 16, 2010, after three months of recording. In addition, swath bathymetry data and very-high-resolution mud-penetrator seismic imagery were collected along the track lines during the HAITI-OBS campaign, to allow better location of the OBS and to enhance the structural framework of the Southern Peninsula.

3. Morphological and Structural Data

[4] An analysis of the detailed swath bathymetry data and the seismic information from the HAITI-OBS cruise in this area shows a rough and tectonically fresh morphology (Figure 1b). The most notable feature is a roughly rhomboidal depression, the Gonâve Basin, with the northwestern edge corresponding to a southeastward hanging N50° normal fault, and with the southern edge bounded by an approximately 70° steep south-dipping N120° reverse fault, the Trois-Baies Fault [*Bien-Aimé Momplaisir*, 1986], which is part of the transpressive flower structure of the EPGFZ. The freshness of this fault on the bathymetry and the presence of recent massive landslides along the scarp clearly show that the fault was active recently; however, we cannot determine whether this activity is related to the January 12, 2010, rupture, or if it is only a recent deformation. The northeastern boundary of the Gonâve Basin shows an asymmetric morphology, in agreement with an interpretation of a blind thrust in front of a ramp anticline that propagates southwestwards. Massive landslides, with several seaward-dipping, lens-shaped features, are frequent on this northern slope. Mud-penetrator data show that although most of these are recent, they are not at present active, with the exception of a slope failure that is observed between Gonâve Island and Rochelois Bank, at W73°05-N18°43, at a depth of approximately 1,000 m. This slope failure reveals the local steepening of the permanent slope and the tilting of the island in a compressive pattern, due to the active deformation of the Gonâve anticline. The eastern edge of the basin is blanketed by the sediments of the fan of the Léogâne Plain. These morphological features show that the present oblique convergence between the Southern Peninsula oceanic block and the main Hispaniola block is partitioned between an E-W left-lateral displacement along the EPGFZ, and a southwestward shortening that includes both north-verging wrench faults, including the Trois-Baies fault, and south-verging blind-thrust faults and folds. These reverse faults inferred here from the tectonic arguments and the high-resolution bathymetry would correspond to the "Léogâne fault" proposed by *Calais et al.* [2010] on the basis of GPS and interferometric data.

4. Large Aftershock Focal Solutions

[5] To calculate the focal mechanisms of some of the larger aftershocks that occurred from January 13 to March 1, 2010 (see Table S1 in the auxiliary material), we modeled the broadband data at regional distances.[1] Data from the Caribbean network were retrieved from the Incorporated Research Institutions for Seismology (IRIS) data center (http://www.iris.edu/wilber) for distances lower than 5°, with the selection defined by an acceptable signal-to-noise ratio in the 0.02 Hz to 0.04 Hz frequency band. This included data from the SDDR (Dominican Republic), MTDJ (Jamaica), GTBY (Cuba) and GRTK (Turks and Caicos Islands) stations. Using the discrete-wave-number method [*Bouchon*, 1981] and the neighborhood algorithm [*Sambridge*, 1999], we determined the parameters that best explained the broadband waveforms: the focal mechanism, seismic moment, hypocenter position and one-dimensional velocity model. As previously noted [*Nettles and Hjörleifsdóttir*, 2010], the resulting focal mechanisms that are presented in Figure 1b show pure reverse motion, which corresponds to N-S to N30° compression, and which is in good agreement with what we observed in the surface deformation, on the land in southern Haiti, and in our detailed bathymetry data. Only one event located near to the main shock epicenter showed a strike-slip movement on a vertical plane.

5. Aftershock Distribution From the Temporary Local Network

[6] Data from our offshore and land seismic stations were processed using an automatic trigger based on the short-time average/long-time average (STA/LTA) algorithm [*Allen*, 1978]. For the OBS, the trigger was applied to both the vertical and the pressure channels, with the latter generally offering a better signal-to-noise ratio. Adequate filtering and a trigger level were selected for the OBS data (4.5 Hz sensors) and land-station data (CMG40 sensors). Applying these to

[1] Auxiliary materials are available in the HTML. doi:10.1029/2011GL049799.

Figure 1. (a) Tectonic and morphological setting of the study area. JAM, Jamaica; D.R., Dominican Republic; P.R., Puerto Rico; EPGFZ, Enriquillo-Plantain Garden Fault Zone; CAR, Caribbean Plate (blue), NOAM, North American Plate (green). (b) Detail of the study area. The focal solutions of the aftershocks from the PDE catalog (first two weeks after the earthquake; see Table S1 in the auxiliary material) are in white/red. The solutions are constrained to be double coupled; yellow circles, three events located in the PDE catalog during the same period as our local network (February 22 09h36, Mw = 4.6; February 23 06h26, Mb = 4.8, and March 1 10h37, Mb = 4.6); grey circles, epicentral location using our local temporary network; S1 and S2, locations of the interpretative cross-sections of Figure 4; yellow star, mainshock location proposed in the present study; yellow box, area illustrated in Figure 1c. (c) Detailed interpretation from multibeam bathymetry of the Gonâve Basin and Léogâne fan.

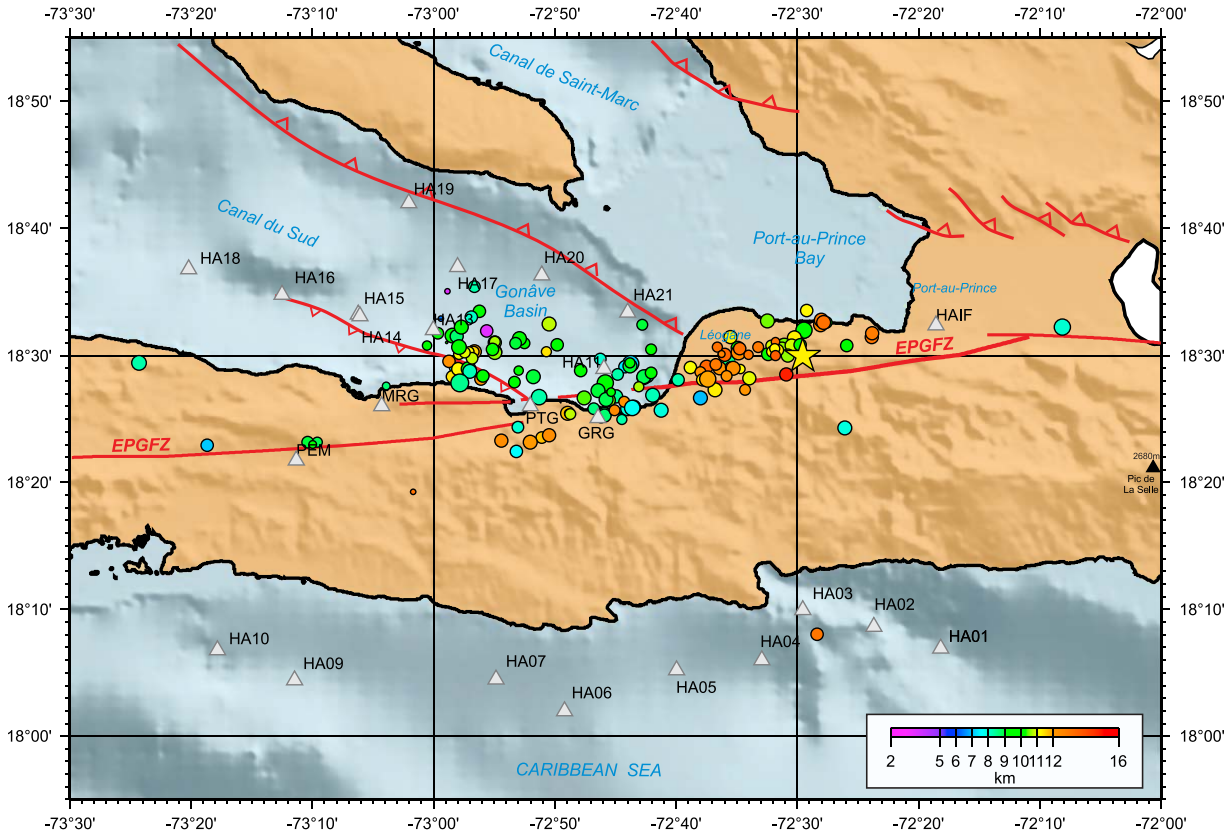

Figure 2. Distribution of the aftershocks observed during the period from February 14 to March 1, 2010. The sizes of the circles are proportional to the coda magnitude determined from the land and OBS records, and the color scale indicates the depths (color scale, bottom-right). Triangles, temporary stations (OBS and land stations); red, surface trace of the EPGFZ; yellow star, mainshock location proposed in the present study (Data listed in Table S3 in the auxiliary material.)

the three weeks of recordings (February 12 to March 7, 2010), we extracted 4,500 time windows where a signal was detected by more than nine stations. Among these time windows, only 25% correspond to events that can be located. The number of detections per day increased after the occurrence of the larger magnitude 4.5 aftershocks on February 22 and March 1, 2010, and also on March 3, 2010. A set of events was picked manually, with priority given to large events. The events were located in the best one-dimensional model, with a constant Vp/Vs ratio (see Table S2 in the auxiliary material], and taking into account the altitude/depth of each recorder. S waves are clearly seen for a large set of events, both onshore and offshore, and the S residuals at the seafloor stations can reach 1 s or more. This suggests the presence of a significant superficial layer, in which the Vp/Vs ratio is very large, and which will generally consist of unconsolidated sediments [*Hirata et al.*, 1989]. As the S waves are important to control the event depth, characterization below each OBS site will be necessary as part of a future study, to improve the S residuals and to reduce the uncertainties of the depth estimation. We obtained 130 epicenters with more than 10 P-wave readings. The horizontal uncertainty is generally smaller than 3 km (except in the eastern part, where the station cover is poor). This distribution gives a good idea of the actual activity during this period, as it corresponds to the largest events. This activity is concentrated mainly to the north of the EPGFZ, with an E-W extent of about 65 km; the western part was very active in the first weeks after the main event (following the National Earthquake Information Center [NEIC] events), and appears to be less active during the period covered, whereas there is strong activity just along the coast near Léogâne. The three large aftershocks located by the NEIC during the same period have epicenters shifted by about 20 km to the NE in our study (Figure 1b). This offset concerns only the three events that were large enough to be recorded by the global network during the same period as our local network, but it is very coherent; we propose that this offset can be applied to the locations of the other aftershocks located by the NEIC during the first month after the main event, on the basis of the permanent seismological networks. The final event distribution (Figure 2) shows some characteristic features: the focal depths range from 7 km and 13 km, and almost all of the activity is located north of the surface trace of the EPGFZ fault. The activity is organized into three clusters that are distributed E-W. The two eastern clusters are sharply limited southwards by the EPGFZ surface trace, and their N-S extent is less than 20 km. The easternmost cluster, which is at the intersection between the EPGFZ and the Transhaitian Belt front, has slightly deeper epicenters. The third cluster, which is on the western part, is more scattered below the Gonâve Basin, and was the most active cluster during the first month of the sequence.

6. Mainshock First-Order Modeling

[7] We modeled the mainshock by a finite fault model (Figure 3) that was constrained using broadband seismological records at teleseismic and regional distances, and

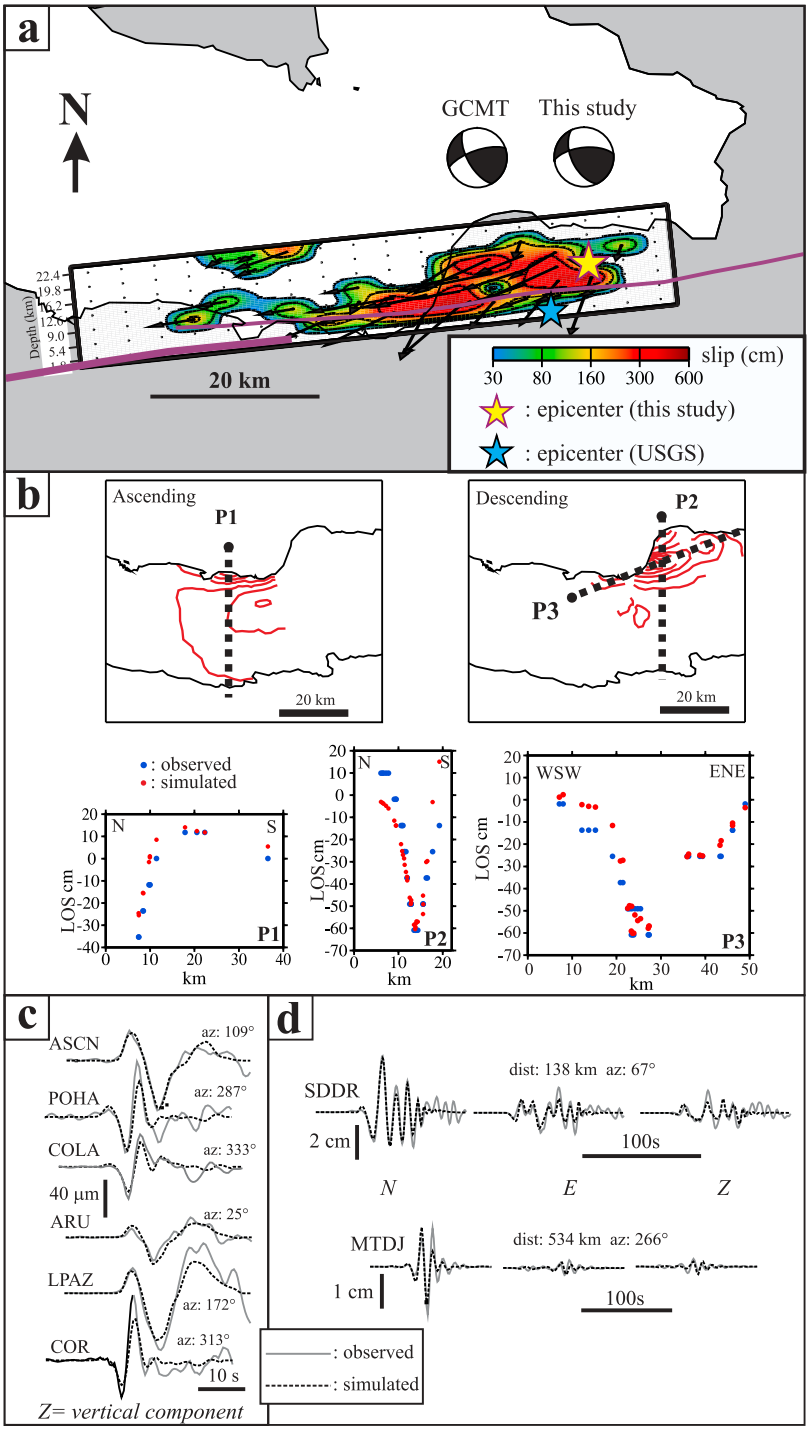

Figure 3. (a) Result of the joint inversion of the seismological and InSAR (© Japan Aerospace Exploration Agency and Ministry of Economy, Trade and Industry of Japan, see text) data for the Haiti main shock. The rectangular finite-fault model is projected onto the surface. Black arrows, direction of motion of the hanging wall with respect to the footwall. The focal mechanism (double-couple component) of the mainshock from the GCMT [*Nettles and Hjörleifsdóttir*, 2010] and from the present study (strike, dip, rake, 264°, 64°, 37°, respectively) are also shown. Yellow star, point of rupture initiation (hypocenter). (b) Different frames illustrating comparisons between the observed and simulated data. Upper panels: red lines, fringes of the two SAR interferograms; heavy dashed lines, two North-South profiles, P1 and P2. The agreement with the line-of-sight (LOS) displacements along these two profiles is also shown. Lower panels: illustrations of the modeling of the seismic records. (c) Teleseismic P-wave displacements (Z, vertical component) at stations ASCN, COLA, POHA, ARU, LPAZ, COR. (d) Three components (N, E, and Z, vertical) of the complete displacement waveforms at regional-distance stations MTDJ (Jamaica) and SDDR (Dominican Republic).

using interferometric synthetic aperture radar (InSAR) data. In total, the data from 33 broadband stations of the Federation of Digital Seismograph Network (FDSN) were retrieved from the IRIS data center (http://www.iris.edu/wilber). Two advanced land-observing satellite/phased array Type L-band synthetic aperture radar (ALOS/PALSAR) interferograms, one ascending (path 138, February 28, 2009–January 16, 2010) and one descending (path 447, March 9, 2009–January 25, 2010), each of which partially covered the rupture zone, were processed and released by the Japan Aerospace Exploration Agency and Ministry of Economy, Trade and Industry of Japan. The finite fault modeling of teleseismic body waves (*P* and *SH*) constrains the strike (264°), dip (64°), and initial rake (43°) of the single rectangular fault-plane solution. The strike agrees with the trend of the EPGFZ and with the elongation axis of the InSAR fringes. The dip of 64° to the North, agrees with the preliminary distribution of aftershocks; on the other hand, this is at odds with the near-vertical dip expected from the linear trend of the EPGFZ. The oblique rake angle also implies a large deviation from the left-lateral motion expected for the EPGFZ. The positioning of the fault model was determined by optimizing the modeling of the InSAR data, with the top of the model at the surface. The slip distribution in space and time is obtained from a joint inversion of the seismological and InSAR data, following the approach described by *Delouis et al.* [2002]. The USGS epicenter is clearly not compatible with the rupture plane dipping to the North. In the absence of local seismic stations, the epicenter determined with the global network can be erroneous by several kilometers. Accordingly, we explored new hypocenter positions in a series of trial-and-error joint inversions. An optimal fit of the joint datasets was obtained with the rupture initiation (the hypocenter) shifted 7 km to the NE with respect to the USGS location. Interestingly, this correction of the location agrees well with the aftershock sequence, as most of the major aftershocks have been located NE of their NEIC epicenter (Figure 1b). The resulting slip distribution is shown in Figure 3, together with a comparison between a subset of observed and simulated data. The rupture propagated unilaterally towards the West, with an average rupture velocity of 2.6 km.s^{-1}. The main slip zone has slip values between 2 m and 5 m, and extends for about 40 km. The absence of significant slip in the uppermost part of the model, which is a result of the inversion because we did not constrain the slip to taper to zero near to the surface, agrees with the lack of clear coseismic offsets observed at the surface. Near to the rupture initiation and in the upper part of the slip distribution, the reverse component is predominant. In the deeper part of the model and in the west, left-lateral slip predominates (Figure 3). The final average rake angle in the model is 37°, and the total seismic moment is $4.9e^{+19}$ N.m, corresponding to Mw = 7.1. The deep slip patch at the northwestern end of the rupture (Figure 3) accounts for less than 5% of the variance reduction; it is thus not likely to be a real feature. The hypocenter depth is constrained by the teleseismic data, as in the range of 12 ± 4 km. Therefore, the NEIC epicenter is incompatible with a north-dipping plane because a rupture plane containing the hypocenter would be too deep under the northern coastal area of the Southern Peninsula, which is in disagreement with the sharp gradient of the displacement field shown by the InSAR data. Only a south-dipping plane, as proposed by *Hayes et al.* [2010], can reconcile the NEIC epicenter with the mainshock rupture. However, with the corrected epicenter, a complex rupture model like the one proposed by *Hayes et al*. [2010] that has fault segments changing in azimuth and dip direction, does not appear to be necessary to satisfactorily explain the first-order characteristics of the seismological and InSAR data. *Hashimoto et al.* [2011] reported an optimal dip of 42° to explain the InSAR data. However, we have verified that such a low dip produces reverse polarities or large amplitude mismatches in the initial parts of the seismograms at many of the teleseismic stations. We show here that the ALOS data are tolerably compatible with a steeper rupture plane, which is in agreement with the seismological data. A possible explanation for the differences in dip found by these two studies might be related to a certain amount of post-seismic deformation that is included in the InSAR data.

7. Discussion

[8] The mechanisms of the aftershocks are pure reverse, or much less frequently, strike-slip (Figure 1), as noted before by *Nettles and Hjörleifsdóttir* [2010], and the strikes are all compatible with the regional stress regime, and in agreement with the full partitioning hypothesis [*Dixon et al.*, 1998; *Calais et al.*, 2002]. Recent studies have modeled a north-dipping fault for the mainshock [*Calais et al.*, 2010; *Hayes et al.*, 2010; *Hashimoto et al.*, 2011], which includes most of the observed slip, with a composite behavior combining reverse and left-lateral components. *Calais et al*. [2010] suggested that this fault, the "Léogâne Fault", is the southern-most thrust of the Transhaitian belt. The geometry of our main shock model shows a very steep (64° to the north) N84°E plane, and a 3 km- to 18 km-deep slip, without surface rupture, which is in good agreement with field observations [*Prentice et al*., 2010]. The slip distribution on this plane shows mainly reverse motion close to the surface, and mainly left-lateral strike-slip in the deeper parts. This plane is unusually steep for a blind frontal thrust in a model of fold-and-thrust sequence, and significantly oblique to the other active or recent N120°E thrust of the Transhaitian Belt. On the eastern part of the affected area, below Léogâne Plain and Petit-Goâve, the aftershocks are distributed on a roughly N75°E direction, at a depth of 9 km to 13 km, below two segments of the EPGFZ. The aftershock distribution has a sharp limit a few kilometers south of the surface trace of the EPGFZ, which is in agreement with a steep south-dipping geometry for the EPGFZ, as suggested by the seismic data [*Bien-Aimé Momplaisir*, 1986]. Therefore, the EPGFZ appears to have an important role, at least as a mechanical boundary after the earthquake. In contrast, the N120°E azimuth of the focal plane of the mechanisms of the aftershocks (Figure 1b), which are mostly of reverse character, are parallel to the azimuth of the Transhaitian Belt; this suggests a triggering of these discontinuities after the earthquake. If we consider that the epicenters determined by the NEIC in the time period separating the mainshock and our survey might be shifted to the NE, the western-most group of aftershocks located below Gonâve Basin, farther north from the trace of the EPGFZ, would reflect the triggering of slip on planes either of the frontal, blind, north-dipping fault of the Transhaitian Belt, or of mechanically compatible steep south-dipping faults, such the Trois-Baies active submarine fault [*Bien-Aimé Momplaisir*, 1986].

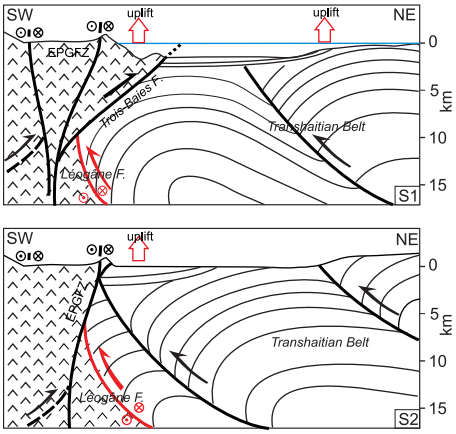

Figure 4. Interpretative cross-sections, as indicated in Figure 1b. (top) S1: Western section, across the Gonâve Basin, showing the Trois-Baies Fault, part of the flower structure of the EPGFZ. (bottom) S2: Eastern section, across the Léogâne Plain and Port-au-Prince Bay. Red, proposed activated fault segment for the January 12, 2010, earthquake. Note: the direction of the Léogâne Fault (N75°E) is significantly oblique to the direction of the Transhaitian Belt and the Trois-Baies faults (N120°E).

[9] Our results clearly show that this Haiti earthquake activated several faults that belong to a secondary fault system that is different from the main EPGFZ, by mainly taking into account the reverse component of the movement (Figure 4). These observations, as well as the surface geometry on the Gonâve Bay area, are in agreement with a model of oblique collision: the rigid thickened oceanic Caribbean crust of the Southern Peninsula/Beata Ridge tends to obliquely under-thrust the mainly sedimentary wedge of the Transhaitian Belt, the western prolongation of the submarine Muertos belt. In such a tectonic context, we assume that the rupture occurred at the rheological boundary above the under-thrust rigid oceanic block (the Léogâne Fault), whereas the aftershocks are the result of the relaxation on the hanging wall of this fault, of the Transhaitian Belt, and along the wrench faults associated with the EPGFZ.

[10] **Acknowledgments.** This study was made possible through the support of INSU, CNRS, IRD and IFREMER. We are grateful to FDSN for public access to global data, to NEIC for monitoring the Caribbean network and for their public release of these data, and to IRIS for easy access to the waveforms. We thank the Captain and the crew of the R/V L'Atalante for their efficiency during the Haiti-OBS cruise, all of the people in charge of the seismological instruments deployed, Jean-David Nagau for part of the picking, and Guust Nolet for useful comments. Special thanks go to Meredith Nettles, for the her comprehensive review of a first version of the paper, which was very helpful to substantially clarify the final contents.

References

Allen, R. V. (1978), Automatic earthquake recognition and timing from single traces, *Bull. Seismol. Soc. Am.*, *68*, 1521–1532.

Bien-Aimé Momplaisir, R. (1986), Contribution à l'étude géologique de la partie orientale du Massif de la Hotte (Presqu'île du Sud d'Haïti): Synthèse structurale des marges de la presqu'île à partir de données sismiques, Ph.D. thesis, 210 pp., Univ. Pierre-et-Marie-Curie (Paris VI), Paris.

Bouchon, M. (1981), A Simple Method to Calculate Green's Functions in Elastic Layered Media, *Bull. Seismol. Soc. Am.*, *71*, 959–971.

Calais, E., Y. Mazabraud, B. Mercier de Lépinay, P. Mann, G. Mattioli, and P. Jansma (2002), Strain partitioning and fault slip rates in the northeastern Caribbean from GPS measurements, *Geophys. Res. Lett.*, *29*(18), 1856, doi:10.1029/2002GL015397.

Calais, E., A. Freed, G. Mattioli, F. Amelung, S. Jónsson, P. Jansma, S.-H. Hong, T. Dixon, C. Prépetit, and R. Momplaisir (2010), Transpressional rupture of an unmapped fault during the 2010, Haiti earthquake, *Nat. Geosci.*, *3*, 794–799, doi:10.1038/ngeo992.

Delouis, B., D. Giardini, P. Lundgren, and J. Salichon (2002), Joint inversion of InSAR, GPS, teleseismic and strong motion data for the spatial and temporal distribution of earthquake slip: Application to the 1999 Izmit mainshock, *Bull. Seismol. Soc. Am.*, *92*, 278–299, doi:10.1785/0120000806.

Dixon, T. H., F. Farina, C. DeMets, P. Jansma, P. Mann, and E. Calais (1998), Relative motion between the Caribbean and North American plates and related boundary zone deformation from a decade of GPS observations, *J. Geophys. Res.*, *103*, 15,157–15,182, doi:10.1029/97JB03575.

Hashimoto, M., Y. Fukushima, and Y. Fukuhata (2011), Fan-delta uplift and mountain subsidence during the Haiti 2010 earthquake, *Nat. Geosci.*, *4*, 255–259, doi:10.1038/ngeo1115.

Hayes, G. P., et al. (2010), Complex rupture during the 12 January 2010 Haiti earthquake, *Nat. Geosci.*, *3*, 800–805, doi:10.1038/ngeo977.

Hirata, N., T. Kanazawa, K. Suyehiro, T. Iwasaki, and H. Shimamura (1989), Observations of microseismicity in the southern Kuril Trench area by arrays of ocean bottom seismometers, *Geophys. J. Int.*, *98*(1), 55–68, doi:10.1111/j.1365-246X.1989.tb05513.x.

Manaker, D. M., E. Calais, A. M. Freed, S. T. Ali, P. Przybylski, G. Mattioli, P. Jansma, C. Prépetit, and J.-B. de Chabalier (2008), Interseismic plate coupling and strain partitioning in the northeastern Caribbean, *Geophys. J. Int.*, *174*, 889–903, doi:10.1111/j.1365-246X.2008.03819.x.

Mann, P., E. Calais, J.-C. Ruegg, C. DeMets, P. E. Jansma, and G. S. Mattioli (2002), Oblique collision in the northeastern Caribbean from GPS measurements and geological observations, *Tectonics*, *21*(6), 1057, doi:10.1029/2001TC001304.

McHugh, C., L. Seeber, N. Braudy, M.-H. Cormier, M. Davis, N. Dieudonne, J. Deming, J. Diebold, R. Douilly, S. Gulick, M. Hornbach, H. Johnson, K. Mishkin, C. Sorlien, M. Steckler, S. Symithe, and J. Templeton (2011), Offshore sedimentary effects of the 12 January Haiti earthquake, *Geology*, *39*(8), pp. 723–726, doi:10.1130/G31815.1.

Nettles, M., and V. Hjörleifsdóttir (2010), Earthquake source parameters for the 2010 January Haiti main shock and aftershock sequence, *Geophys. J. Int.*, *183*, 375–380, doi:10.1111/j.1365-246X.2010.04732.x.

Prentice, C. S., P. Mann, A. J. Crone, R. D. Gold, K. W. Hudnut, R. W. Briggs, R. D. Koehler, and P. Jean (2010), Seismic hazard of the Enriquillo–Plantain Garden fault in Haiti inferred from palaeoseismology, *Nat. Geosci.*, *3*, 789–793, doi:10.1038/ngeo991.

Pubellier, M., A. Mauffret, S. Leroy, J.-M. Vila, and H. Amilcar (2000), Plate boundary readjustment in oblique convergence: Example of the Neogene of Hispaniola, Greater Antilles, *Tectonics*, *19*, 630–648, doi:10.1029/2000TC900007.

Sambridge, M. (1999), Geophysical inversion with a neighbourhood algorithm. I. Searching a parameter space, *Geophys. J. Int.*, *138*, 479–494, doi:10.1046/j.1365-246X.1999.00876.x.

M.-P. Bouin, Observatoire Volcanologique et Sismologique de la Guadeloupe, Institut de Physique du Globe de Paris, 97113 Gourbeyre, Guadeloupe.

P. Charvis, B. Delouis, A. Deschamps, Y. Hello, B. Mercier de Lépinay, and M. Vallée, Géoazur, CNRS, Université de Nice, IRD, 250 rue A. Einstein, F-06560 Valbonne CEDEX, France. (bmercier@geoazur.unice.fr)

V. Clouard and J.-M. Saurel, Observatoire Volcanologique et Sismologique de la Martinique, Institut de Physique du Globe de Paris, 97250 Fonds-St-Denis, Martinique.

J. Crozon and F. Klingelhoefer, Géosciences Marines, Ifremer, BP 70, F-29280 Plouzané CEDEX, France.

D. Graindorge and J. Perrot, IUEM, Université de Bretagne Occidentale, Place Nicolas Copernic, F-29280 Plouzané CEDEX, France.

B. Marcaillou and Y. Mazabraud, IUFM de Guadeloupe, Université Antilles-Guyane, Campus de Fouillole, BP 592, 97159 Pointe-à-Pître, Guadeloupe.

M. St-Louis, Bureau des Mines et de l'Energie, Delmas 19, Rue Nina 14, Box 2174, Port-au-Prince, Haiti.